Springer

KSME

Journal of Mechanical Science and Technology 33 (7) (2019) 3277~3288
www.springerlink.com/content/1738-494x(Print)/1976-3824(Online)
DOI 10.1007/s12206-019-0623-4

Flapping flight in the wake of a leading insect †

Anh Tuan Nguyen*, Thanh Dong Pham and Quoc Tru Vu

Faculty of Aerospace Engineering, Le Quy Don Technical University, 236 Hoang Quoc Viet, Ha Noi, Vietnam

(Manuscript Received October 21, 2018; Revised February 23, 2019; Accepted March 25, 2019)

Abstract

This study explores the wake effects of an upstream leading insect on the flight performance of a following one. The potential-flow based aerodynamic model, which combines the unsteady panel and unsteady vortex-lattice methods, is used to compute aerodynamic loads and simulate wake structures. The accuracy of the current aerodynamic model was confirmed in this study. The paper shows that the following insect does not cause any noticeable impact on the leading insect aerodynamics, while unfavorable effects due to the presence of the leading insect were found on the following counterpart. Nonetheless, by choosing a proper wing kinematic phase, the following insect may absorb the energy of the leading insect's trailing wake, and therefore mitigate these negative effects. The variations of the required mechanical power of the following insect against the wing kinematic phase difference were shown to be related to the travel of the leading insect's downstroke starting vortex.

Keywords: Insect flight; Wing-wake interaction; Potential-flow theory; Unsteady panel method

1. Introduction

Insects may aerodynamically interact with their flying neighbors when swarming in close proximity. During this flight, an insect may strongly collide with the wakes of others, and this type of problem has not been investigated in previous studies that treated each insect independently [1-4]. When conducting experiments on dynamically scaled insect-like robotic wings, researchers have uncovered some crucial aerodynamic mechanisms, including the delayed stall, wing rotation and wake capture effect [5-8]. More recently, Ortega-Jimenez et al. [9] and Ravi et al. [10] studied the behaviors of hawkmoths and bumblebees in turbulent airflows caused by the von Karman vortex streets behind cylinders; Vance et al. [11] investigated how insects adjust their wing kinematics and body orientations to mitigate gust perturbations. Nonetheless, the experience of flying in the wake of another insect may be totally different from that in the above mentioned studies. First, insect wake shedding is periodic and has a frequency equal to that of the wing motions [12]. Secondly, unlike the von Karman vortex streets in the experiments conducted by Ortega-Jimenez et al. [9] and Ravi et al. [10], unsteady wakes, which are caused by the multi-degree-of-freedom motions of insect wings [13], have more complex structures formed by the trailing-edge, leading-edge, tip and root vortices [12, 14]. It has been shown that the interactions between insects and their own wakes could benefit their lift production [6, 8, 15, 16] and probably affect the dynamic flight stability characteristics considerably [17, 18]. Nevertheless, a physical insight into the interaction between an insect and the wake shed from another one has not been achieved so far.

The effects of wake encounters have been investigated and well documented for fixed-wing airplanes [19, 20]. However, so far, for flapping-wing insects, this type of problem has not been explored despite its significance in nature. In this work, for the first time, the answer to the question of how insect flight performance is affected by the unsteady wake of another one is discussed. Herein, two insects are assumed to fly together at the same flight speed. The upstream leading insect sheds unsteady wakes that travel downstream and interact with the following insect. Aerodynamic loads are computed by an efficient potential-flow based model that combines the unsteady panel method (UPM) and the unsteady vortex-lattice method (UVLM). The leading-edge suction analogy model is incorporated into the present aerodynamic model to include the delayed stall effect. The wakes are modeled by a system of vortex lines that have growing core sizes over time and transport freely with the local velocity of the flowfield. Compared to higher-order methods solving the three-dimensional Navier-Stokes equations, the current aerodynamic model requires much less computation effort, and therefore, becomes more appropriate for the present study, in which a large number of simulations are required for an iterative trim search method. By modifying the wing kinematic phase difference between the two insects, it is possible to observe the variation trend of

*Corresponding author. Tel.: +84 888 000438
E-mail address: anhtuannguyen2410@gmail.com
† Recommended by Associate Editor Seongwon Kang

Table 1. Mass and morphological parameters of the hawkmoth.

m (mg)	1578.70
R (mm)	48.50
$\bar{c}$ (mm)	16.81
S (mm^2)	815.33
r_2	0.53
L (mm)	44.80
l/L	0.45
l_1/L	0.25

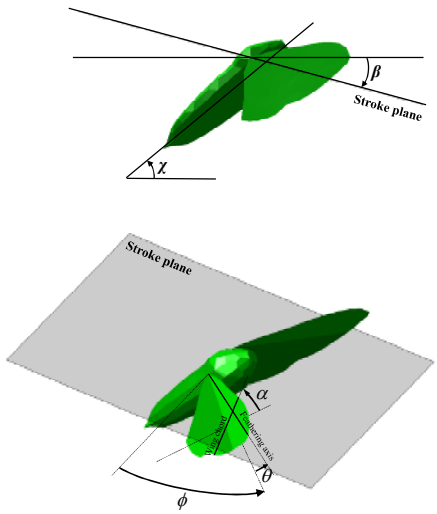

Fig. 1. Insect model and angle definitions.

the following insect's required mechanical power. The velocity fields and wake structures are presented to provide the physical explanations of this trend. Moreover, based on the power variation profile, it is possible to choose an appropriate wing kinematic phase to enhance the flight efficiency of the following insect. In this study, wing kinematic coefficients were tuned to obtain the trim conditions, and the wake effects on these coefficients were also studied.

2. Insect model and methodologies

2.1 Insect model

The leading and following insects are assumed to have the same morphological parameters, which are based on measurement data of the hawkmoth *Manduca sexta* [21, 22]. Some basic parameters of the wings and bodies are given in Table 1, where m is the mass of a hawkmoth; R, $\bar{c}$, S and r_2 respectively, denote the wing span, mean chord length, wing area and radius of the second moment of wing area; L is the length of the body; l and l_1 denote the distance from the center of mass of the body to the anterior tip and that to the wing-base pivot, respectively.

According to Fig. 1, the body angle χ is defined as the angle between the body axis of an insect and the horizontal plane. Wing orientation is determined by the set of three Euler angles ϕ, θ and α relative to the stroke plane, which is inclined at angle β. These Euler angles, respectively, represent the sweep angle, which defines the angular displacement of the wing corresponding to back and forth motions; the elevation angle, which is corresponding to the up and down motions of the wing; and the rotation angle of the wing about its feathering axis.

Willmott and Ellington [13] measured the variations of ϕ, θ and α during one wingbeat stroke of the hawkmoth *Manduca sexta* at various flight speeds. In this paper, for simplicity, the wing motions of the insects are represented by sinusoidal harmonic functions with a frequency f as follows:

$$\begin{aligned} \phi(t) &= \phi_0 + \phi_a \cos(2\pi f t), \\ \theta(t) &= \theta_0, \\ \alpha(t) &= \alpha_0 + \alpha_a \sin(2\pi f t). \end{aligned} \tag{1}$$

The coefficients used in Eq. (1) are determined based on the measurement data from real hawkmoths [13, 23]. However, to obtain the equilibrium flight state, some coefficients have to be adjusted to satisfy the force and moment balance conditions. Note that the small variation of the elevation angle θ, which was observed in previous measurements, is neglected here, and thus, this angle is assumed constant.

2.2 Aerodynamic model

To compute the aerodynamic forces acting on the insect wings and bodies, the UPM and the UVLM are employed, respectively. These methods are based on the potential flow theory, which is applied for irrotational flow fields [24]. The validity of this approach has been proved for several applications, in which viscous effects are ignored. In this study, the aerodynamic model allows the computational program to include some important features of insect aerodynamics, which cannot be treated by conventional potential-flow based models. Specifically, the effect of leading-edge vortices that cause the delayed stall on insect wings [5] can be considered through the leading-edge suction analogy model. Moreover, viscous diffusion is also taken into account by the use of the vortex-core growth model. Compared to higher-order aerodynamic models that directly solve the Navier-Stokes equations, the present aerodynamic model is more efficient because of its substantially lower computational cost, while most of the important effects of insect aerodynamics are still included with a relatively high level of accuracy [25-27]. Particularly, when the parallel computing technique is applied to update the geometry of the free wake after each time step, the running time of the current program may be reduced significantly [26].

Regarding the UPM, which is applied to compute the aerodynamic loads on the insect bodies, it is assumed that the flow is irrotational, inviscid, incompressible and no separation is allowed to occur. The basic idea of this method is to solve the Laplace equation of the velocity potential Φ numerically with

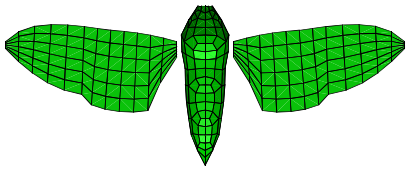

Fig. 2. Aerodynamic panel mesh.

the consideration of three boundary conditions, including the far field, the Neumann and the Dirichlet boundary conditions [24]. These boundary conditions, respectively, guarantee the zero velocity perturbations in the far field, the no-penetration of the flow into the body surfaces, and the constant velocity potential inside the solid bodies.

Following Green's identity, while solving the Laplace equation of the velocity potential Φ, the general solution can be constructed by a sum of source σ and doublet μ distributions on the body surfaces S_b and the wake sheets S_w:

$$\Phi(\boldsymbol{r},t) = -\frac{1}{4\pi}\int_{S_b}\left[\sigma\left(\frac{1}{|\boldsymbol{r}|}\right) - \mu\boldsymbol{n}\cdot\nabla\left(\frac{1}{|\boldsymbol{r}|}\right)\right]dS + \frac{1}{4\pi}\int_{S_w}\mu\boldsymbol{n}\cdot\nabla\left(\frac{1}{|\boldsymbol{r}|}\right)dS. \tag{2}$$

Here, $\boldsymbol{r}$ is the position vector, $\boldsymbol{n}$ denotes the unit outward normal vector.

According to the Neumann boundary condition, which is corresponding to the no-penetration condition of the flow, the source σ is determined as

$$\sigma = \boldsymbol{V}_b \cdot \boldsymbol{n}, \tag{3}$$

where $\boldsymbol{V}_b$ is the velocity of a body.

The doublet μ can be defined as the difference between the internal and external velocity potentials in the case of solid bodies (Eq. (4)), and between the lower and upper surfaces in the case of wake sheets (Eq. (5)):

$$\mu = \Phi_i - \Phi, \tag{4}$$

$$\mu = \Phi_l - \Phi_u. \tag{5}$$

Φ_i denotes the internal velocity potential of a body, and subscripts l and u refer to the lower and upper surfaces of a wake sheet.

To solve the aerodynamic problem numerically, the insects are discretized into panels (Fig. 2), on which source and doublet elements are placed. Collocation points, at which we apply the boundary conditions, are located at the centers of these panels. The strength of the source elements on the insect bodies is determined by Eq. (3), while the strength of the doublet elements is found by solving the system of algebraic equations, which is formed by applying the Dirichlet boundary condition at the collocation points.

For the insect wings, which are considered to be thin objects, the upper and lower surfaces coincide with each other and have the opposite normal unit vectors. Therefore, the source elements, which are determined by Eq. (3) on the upper and lower surfaces of the wings, will cancel each other out. Consequently, it is possible to exclude the source elements on the insect wings. Moreover, due to the equivalence between constant doublet elements and vortex rings, the insect wings could be represented by a system of vortex ring panels, and the UPM will become the UVLM [26, 28]. Thus, the present aerodynamic model couples the UPM and the UVLM, which are used for the bodies and the wings of the insects, respectively. Note that while applying the Dirichlet boundary conditions to the insect bodies, the contributions of the wings and their wakes are included; and similarly, the effect of the bodies on the no-penetration boundary condition of the wings must be considered, too. The Kutta condition is satisfied along the trailing edges of the wings; therefore, vortices are shed freely from these edges to form the free wakes. For the UVLM, the wakes can be represented by a vortex line system with the finite core radius, and the velocity potential caused by the wakes Φ_{wake} at point P can be determined as follows:

$$\Phi_{wake} = \int_{P_\infty}^{P} \boldsymbol{V}_{wake}\, d\boldsymbol{s}, \tag{6}$$

where P_∞ is an arbitrary point in the far field, and $\boldsymbol{V}_{wake}$ denotes the velocity induced by the wakes.

Similar to other potential-flow based methods, in this study, the aerodynamic pressure distributions on the insect bodies are obtained by the unsteady Bernoulli equation:

$$p = p_{ref} - \rho\left[\frac{1}{2}\nabla\Phi\cdot\nabla\Phi + \boldsymbol{V}_{ref}\cdot\nabla\Phi + \frac{\partial\Phi}{\partial t}\right], \tag{7}$$

where p_{ref} and $\boldsymbol{V}_{ref}$ denote the reference pressure and velocity, which are, respectively, set to be equal to the far-field pressure and the relative velocity of the undisturbed fluid with respect to the reference point on an insect body; and ρ is the air density.

For the thin insect wings, the UPM is reduced to the UVLM; thus, Eq. (7) could be changed to a simpler form to compute the pressure difference between the lower and upper surfaces:

$$\Delta p = \rho\left[\left(\boldsymbol{V}_{rel}\times\boldsymbol{\gamma}\right)\cdot\boldsymbol{n} + \frac{\partial\Gamma}{\partial t}\right], \tag{8}$$

where $\boldsymbol{V}_{rel}$ is the velocity of the flow relative to the wing surface; $\boldsymbol{\gamma}$ denotes the local surface vorticity vector; and Γ is the circulation of the local vortex ring.

The total aerodynamic force and moment acting on an insect can be computed by integrating the pressure obtained by Eqs. (7) and (8) over the entire body and wing surfaces.

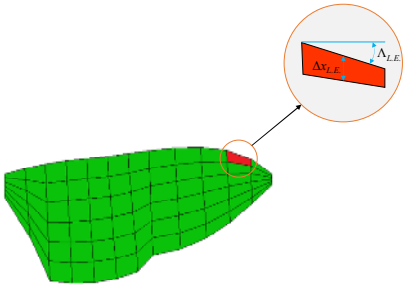

Fig. 3. Leading-edge panel.

Previous authors have emphasized the importance of leading-edge vortices that cause the delayed stall in the high-lift aerodynamic mechanism of insect wings [5, 29]. Thus, it is necessary to include the contribution of this term in the present aerodynamic model. In general, the delayed stall, which is associated with the separation and reattachment of the flow near the leading edge of an insect wing, cannot be treated by the potential-flow theory. However, Polhamus stated that when the delayed stall occurs, the flow around the leading-edge vortex is somewhat similar to the potential flow around the leading-edge radius [30]. Due to this analogy, it is possible to relate the suction force of the potential flow to the vortex force, which appears due to the presence of the leading-edge vortex, and the vortex force per unit length of the leading edge F_v can be estimated as [26]

$$F_v = \frac{\pi}{16}\frac{\eta_s \rho \Gamma_{L.E.}^2}{\Delta x_{L.E.} \cos \Lambda_{L.E.}}, \tag{9}$$

where η_s denotes the coefficient of leading-edge suction efficiency; $\Gamma_{L.E.}$ is the circulation of the vortex segment placed at the leading edge; and $\Delta x_{L.E.}$ and $\Lambda_{L.E.}$ are, respectively, the length in the chordwise direction and the sweep angle of the local leading-edge panel, which are illustrated in Fig. 3. According to Nguyen et al. [26], the coefficient of leading-edge suction efficiency η_s is 0.5 for hawkmoth flight.

In general, viscous effects cannot be treated by potential-flow theory; however, the model used in this paper can be modified to include these effects by allowing the core radius of the vortex lines in the free wake to increase over time. This vortex-core growth assumption is based on the observation result by Ramasamy and Leishman [31], who indicated the effect of the viscous diffusion on the core size of vortex lines. The vortex radius r_c of a vortex line with circulation Γ was determined by Nguyen et al. [26], and Gandhi and Tauszig [32] as

$$r_c(t) = \sqrt{4\alpha_L \nu \left(1 + a_1 \frac{\Gamma}{\nu}\right) t}. \tag{10}$$

Here, $\alpha_L = 1.25643$ is the Lamb constant; ν and a_1 are the kinematic viscosity and Squire's parameter, respectively.

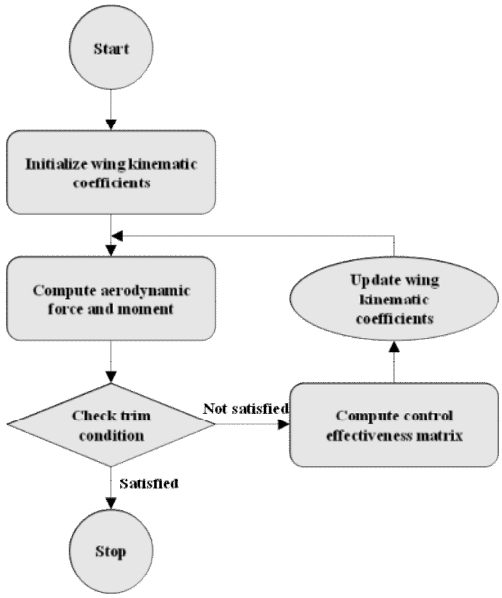

Fig. 4. Scheme of trim search method.

Nguyen et al. indicated that $a_1 = 0.1$ is suitable for modeling the wake generated by a hawkmoth [26].

2.3 Trim search method

In this research, the small oscillations of insect bodies are neglected [13], and the insects are assumed to fly at a constant speed. During trimmed flight, the force and moment balance conditions must be satisfied. As demonstrated by Kim and Han [33], the changes in the sweep angle amplitude ϕ_a, the rotation angle offset α_0 and the sweep angle offset ϕ_0 mentioned in Eq. (1) are the most effective with respect to the controls of the lift, drag and pitching moment, respectively. Thus, to find trimmed flight, these coefficients will be tuned until the balance conditions of the force and moment are satisfied.

Trimmed flight of an insect is obtained by an iterative method that is illustrated in Fig. 4. The initial wing kinematic coefficients for the trim search method are chosen on the basis of the measured hawkmoth wing motions [23]. The trim criteria are satisfied once the resultant force and moment are less than given tolerance values. Here, the tolerance values are the same as those used by Nguyen et al. [4] and Nguyen and Han [34]. In detail, the tolerance for the lift and drag is 1.0 % of the insect weight, and that for the pitching moment is 0.1 % of the product of the weight and the mean wing chord. Nguyen et al. demonstrated that these tolerance values are sufficiently small to assure a trimmed flight state [4]. If the trim criteria are not satisfied, the wing kinematics must be altered. As mentioned, ϕ_a, α_0 and ϕ_0 are three kinematic coefficients that are modified to obtain the trim conditions. A gradient-based method is used to calculate the new coefficients through the control effectiveness matrix **B**, which is defined as

$$\mathbf{B}=\begin{bmatrix} \frac{\partial \bar{L}}{\partial \phi_a} & \frac{\partial \bar{L}}{\partial \alpha_0} & \frac{\partial \bar{L}}{\partial \phi_0} \\ \frac{\partial \bar{D}}{\partial \phi_a} & \frac{\partial \bar{D}}{\partial \alpha_0} & \frac{\partial \bar{D}}{\partial \phi_0} \\ \frac{\partial \bar{M}}{\partial \phi_a} & \frac{\partial \bar{M}}{\partial \alpha_0} & \frac{\partial \bar{M}}{\partial \phi_0} \end{bmatrix}, \tag{11}$$

where $\bar{L}$, $\bar{D}$ and $\bar{M}$ denote the cycle-average lift, drag and pitching moment. It is noted that lift and drag are defined as force components that are perpendicular and parallel to the flight direction of an insect, respectively.

The values of the kinematic coefficients at the k+1th iteration are computed by the following equation:

$$\begin{bmatrix} \phi_a \\ \alpha_0 \\ \phi_0 \end{bmatrix}_{k+1} = \begin{bmatrix} \phi_a \\ \alpha_0 \\ \phi_0 \end{bmatrix}_{k} + \mathbf{B}_k^{-1} \begin{bmatrix} \Delta\bar{L} \\ \Delta\bar{D} \\ \Delta\bar{M} \end{bmatrix}_k . \tag{12}$$

In this equation, $\Delta\bar{L}$, $\Delta\bar{D}$ and $\Delta\bar{M}$ are the offset lift, drag and pitching moment needed to apply to the insect to obtain the balance condition.

First, this method is used to find the trimmed flight conditions of a single insect. When two insects fly together, it will be shown later in this paper that the effect of the following insect on the aerodynamics of the leading counterpart is inconsiderable; hence, the trimmed flight conditions of the leading insect can be considered to be the same as that of a single insect. Consequently, it is required to find only the trim conditions of the following insect.

3. Results and discussion

3.1 Validation of the aerodynamic model

The validity of the current aerodynamic model has been ascertained in several previous papers for hawkmoth-like insect models [4, 26-28]. In this paper, the aerodynamic model is first validated again in comparison with results from computational fluid dynamics (CFD) methods that solve the Navier-Stokes equations directly. Fig. 5 shows the lift forces acting on a wing and the body of a hovering hawkmoth *Agrius convoluli*, a species close to *Manduca sexta*. In this figure, time is normalized with the stroke period. The forces computed by the present aerodynamic model are in good agreement with the CFD results from a study by Aono et al. [35].

Lua et al. [36] conducted an experiment for robotic hawkmoth wings to measure the aerodynamic force in the stroke-plane-fixed reference frame. The wing force in a direction perpendicular to the stroke plane determined by the present model is compared with that obtained through experimental data (Fig. 6). Good consistency between these results can be found in this figure.

The downwash structures simulated by the CFD model [14] and the current aerodynamic model are presented in Fig. 7. In this figure, the downwash velocity is normalized with the mean wing-tip velocity. The similarity between these downwash structures confirms that the vortex-core growth model represented by Eq. (10) is suitable for handling the viscous diffusion effect.

For the present study, it was important to accurately model

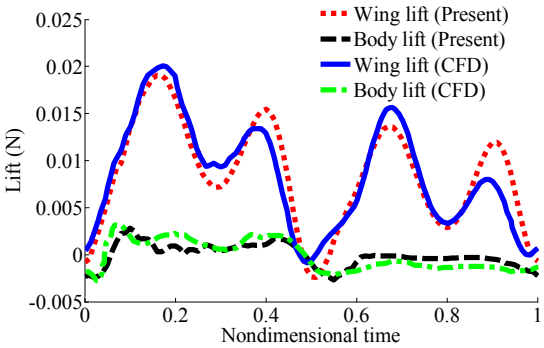

Fig. 5. Lift forces on a wing and the body by the present potential-flow based aerodynamic model and by a CFD modeling method [35].

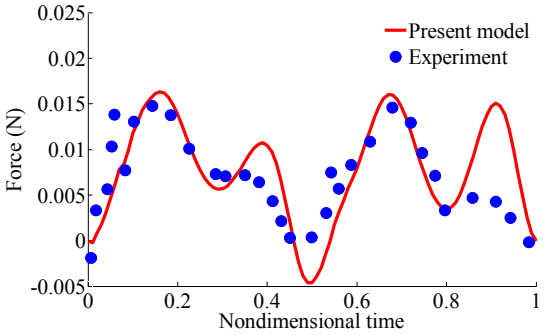

Fig. 6. Wing force in a direction perpendicular to the stroke plane obtained by the present model and from an experiment on robotic hawkmoth wings [36].

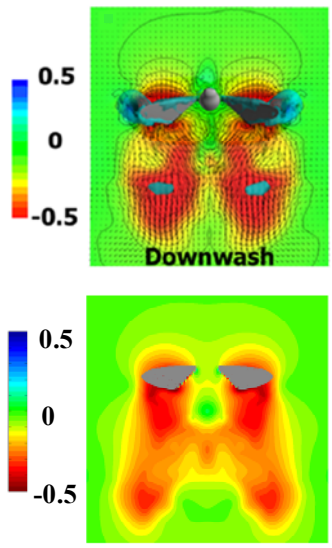

Fig. 7. Downwash structures obtained by the CFD model [14] (up) and by the present aerodynamic model (down).

Table 2. Kinematic parameters.

β (deg)	35.8
χ (deg)	21.7
f (Hz)	25.6
θ_0 (deg)	-8.6
α_a (deg)	46.4

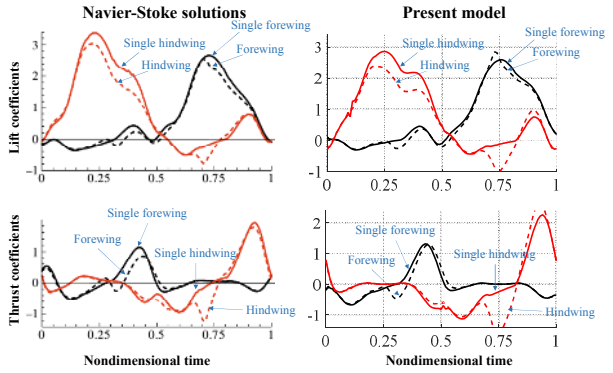

Fig. 8. Time courses of the lift and thrust coefficients on the fore- and hindwings by solving the Navier-Stoke equations [36] and from the present aerodynamic model.

the interaction between the wings of the following insect and the trailing wake of the leading counterpart. It appears that there has not been any previous research on this type of problem. Thus, to investigate the accuracy of the currently employed model in terms of handling strong wing-wake interaction, a similar case of dragonfly aerodynamics was considered. For dragonflies, hindwings collide with the wakes of forewings in a similar manner to that between the following and leading insects. Wang and Sun [37] numerically solved the Navier-Stokes equations to study the aerodynamics of the dragonfly *Aeshna juncea* at a Reynolds number of almost 3000 based on the mean wing-tip velocity, compared to 6000 of hawkmoth flight. The wing lift and wing thrust coefficients of the hovering dragonfly are computed along with those of the single isolated wings and shown in Fig. 8. Here, the force coefficients are calculated based on the mean wing velocity and the total wing area. From a comparison between the results from the two models, it is possible to state that the present potential-based aerodynamic model can reasonably estimate the effect of strong wing-wake interaction. According to Sun and Lan [38], the interaction effect reduces the lift forces on the fore- and hindwings of the hovering dragonfly by 14 % and 16 %, respectively. Using the present aerodynamic model, these values are estimated to be, respectively, 12 % and 20 %.

3.2 Trimmed flight state of a single insect

Initially, the trim search method was applied for a single insect flying at a constant speed of 2.0 m/s, which is considered to be within the favorable flight speed range of hawkmoths

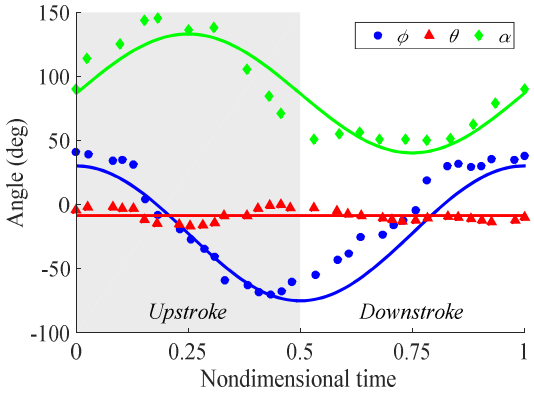

Fig. 9. Trimmed wing kinematics (solid lines) and measurement data from a real hawkmoth [23].

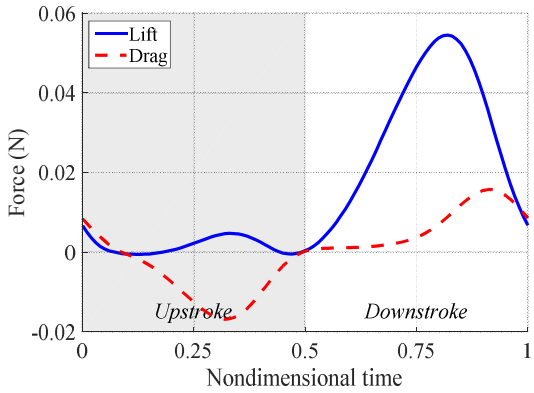

Fig. 10. Lift and drag forces during the course of a wingbeat stroke.

[12]. Table 2 provides the values of the stroke plane angle β, body angle χ, flapping frequency f and some coefficients of the simplified sinusoidal wing kinematics expressed in Eq. (1). These flight parameters are given based on the measured data from a male hawkmoth at 2.0 m/s [23].

As mentioned in Sec. 2.3, the sweep angle amplitude ϕ_a, the rotation angle offset α_0 and the sweep angle offset ϕ_0 are tuned during the trim search process. After obtaining the trim solution for a single insect, the wing kinematic functions are plotted and compared with the measurement data from a real hawkmoth [23] in Fig. 9. The figure shows good agreement between the trimmed wing kinematics (solid lines) and the measurement data (markers).

The lift and drag of the insect during the course of a wingbeat stroke are shown in Fig. 10. The variation of the lift has a much larger peak-to-peak amplitude than that of the drag. Most of the lift is produced during the downstroke phase of the wing motion.

The required mechanical power during the trimmed flight can be estimated as the sum of its three components P_ϕ, P_θ and P_α corresponding to the sweeping, elevating and rotating motions of the wings. According to Casey [39], the contribution of the elastic storage mechanism to the total mechanical power of hawkmoths is insignificant. Therefore, it is possible to assume that the negative power is simply dissipated

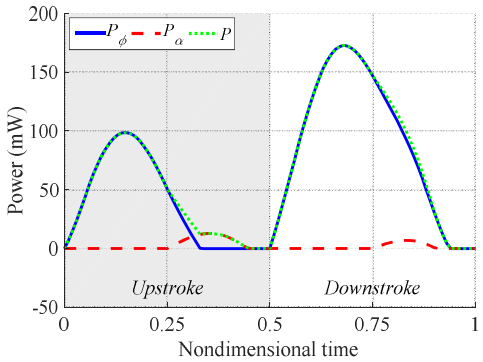

Fig. 11. The total required mechanical power P and its components P_ϕ and P_α.

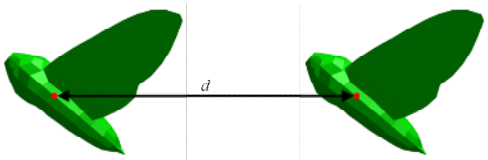

Fig. 12. The leading and following insects and the distance between them.

and the flight muscles act as an end stop [40]. The power components can then be calculated as

$$P_j = \tau_j \frac{dj}{dt} \qquad if\left(\tau_j \frac{dj}{dt} > 0\right),$$
$$P_j = 0 \qquad if\left(\tau_j \frac{dj}{dt} \le 0\right), \qquad (13)$$
$$\left(j = \phi, \theta, \alpha\right),$$

where τ denotes the torque required to overcome the inertial and aerodynamic forces acting on the wings.

The total mechanical power P and its components P_ϕ and P_α are exhibited in Fig. 11. Note that P_θ is 0 since the variation of the elevation angle θ is neglected, and this angle is held constant. Similar to the aerodynamic forces, the required mechanical power during the downstroke is more significant than that during the upstroke. The mean mechanical power for the trimmed flight of a single insect is estimated to be 65.7 mW.

3.3 Flight of the following insect in the wake of the leading insect

This section presents some numerical results to reveal how the interactions between insects can affect their flight performance. Two insects, which have the same flight speed of 2.0 m/s, are positioned as shown in Fig. 12. The distance d between the mass centers of the two insects varies from 100 mm to 175 mm, corresponding to from 2.2 to 3.9 times of the body length.

At first, the two insects are assumed to have the wing kinematics of a trimmed single insect, as derived in Sec. 3.2. Two

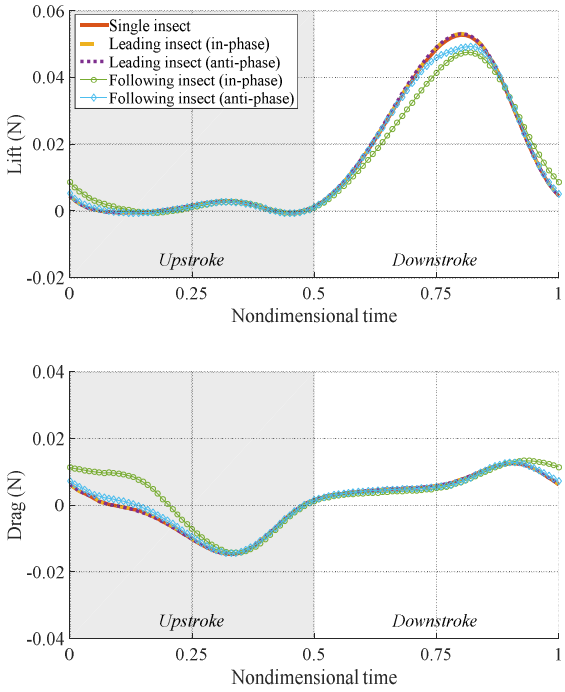

Fig. 13. Lift and drag forces on the leading and following insects in cases of in-phase and anti-phase wing motions.

cases, including the in-phase and anti-phase wing motions, are considered. The anti-phase case is corresponding to a phase difference of 50 % of the stroke period between the two insects. The lift and drag forces of the leading and following insects at a distance d of 100 mm are shown in Fig. 13. It is easy to find that there is almost no change in the aerodynamic force acting on the leader due to the presence of the follower in both in-phase and anti-phase cases. Hence, the trim conditions and the required mechanical power of the leading insect can be regarded as unchanged and assumed to be the same as those of a single insect. This statement becomes even more valid at a larger distance d.

On the contrary, Fig. 13 indicates that the leading insect has considerable effects on the lift and drag of the following insect. These effects tend to be dependent on the wing kinematic phase relationship. In general, due to the induced downwash produced by the leading insect, the lift of the following insect decreases, while the drag appears to increase because of an airflow that is pushed backward by the leader to generate thrust.

Next, the trim search method runs for the following insect for various values of the distance d and the phase difference. As presented earlier, three coefficients of the wing kinematics, including the sweep angle amplitude ϕ_a, the rotation angle offset α_0 and the sweep angle offset ϕ_0 (Eq. (1)), are adjusted to obtain the trimmed flight state of the insect. After running the trim search program, the variations of these coefficients and the required mechanical power against the wing kinematic phase shift of the follower relative to the leader are plotted and shown in Figs. 14-17. The plots in these figures

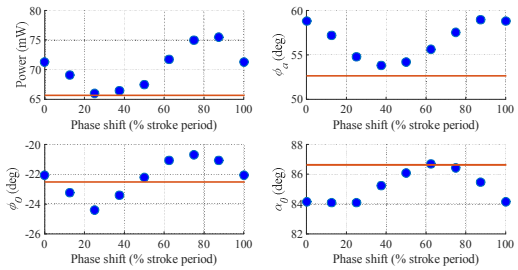

Fig. 14. Required mechanical power and wing kinematics coefficients of the following insect in trimmed flight against the phase shift of the wing motions when the distance *d* equals 100 mm. Solid lines show the values for the single insect.

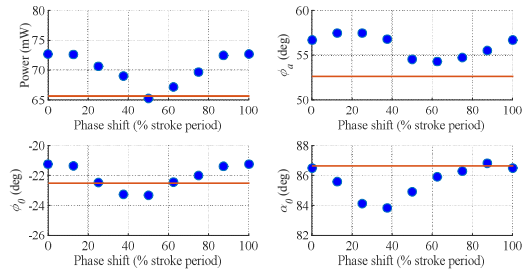

Fig. 15. Required mechanical power and wing kinematics coefficients of the following insect in trimmed flight against the phase shift of the wing motions when the distance *d* equals 125 mm. Solid lines show the values for the single insect.

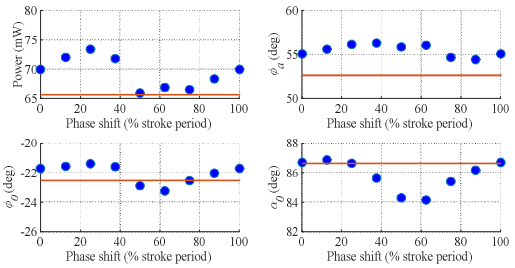

Fig. 16. Required mechanical power and wing kinematics coefficients of the following insect in trimmed flight against the phase shift of the wing motions when the distance *d* equals 150 mm. Solid lines show the values for the single insect.

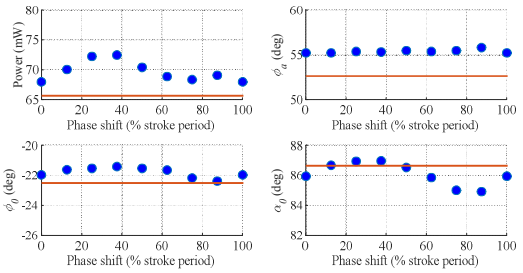

Fig. 17. Required mechanical power and wing kinematics coefficients of the following insect in trimmed flight against the phase shift of the wing motions when the distance *d* equals 175 mm. Solid lines show the values for the single insect.

are corresponding to distances *d* of 100, 125, 150 and 175 mm, respectively.

As can be seen in Figs. 14-17, flying in the wake of the upstream leading insect generally reduces the efficiency of the follower since more mechanical power is required. The power requirement significantly depends on the phase shift of the following insect's wing kinematics. Therefore, at each distance, by choosing a proper wing kinematic phase, the following insect can attenuate the unfavorable effects due to the presence of the leading one, as well as enhance the flight efficiency considerably. For example, at a distance of 100 mm (Fig. 14), amongst the nine considered cases, the required power achieves the largest value of 75.5 mW at a phase shift of 87.5 % of the stroke period. This amount is about 15 % larger than that required for single insect flight. However, if the insect changes its wing kinematic phase shift to 25 % of the stroke period, the required power decreases to 66.0 mW, which is close to the level of the single insect.

Similar to the mechanical power, the wing kinematic coefficients also depend on the phase relationship between the two insects. Figs. 14-17 show that the sweep angle amplitude ϕ_a of the following insects tends to be larger than that of the single insect. This finding can be explained by the existence of the induced downwash generated by the leading insect, which is detrimental to the lift production of the follower. Kim and Han revealed that the change in the sweep angle amplitude is the most effective in terms of lift force control [33]. Therefore, to mitigate the adverse effects of the downwash on the lift production, the following insect has to increase its sweep angle amplitude ϕ_a. Nguyen et al. showed that at 2.0 m/s, the drag of the hawkmoth is sensitive to the change in the velocity of the incoming airflow [4]. The leading insect has to push air backward to create thrust; thus, it will magnify the intensity of the incoming airflow to the following insect and result in an increase in the drag of this insect. Consequently, to maintain the force balance condition, the following insect has to fly at a smaller angle of attack during the downstroke by reducing the rotation angle offset α_0 [33]. This trend can be clearly observed in Figs. 14-17 when the rotation angle offset α_0 is lower than that of the single insect in almost all cases. Nguyen et al. [4] also indicated that both downward and backward airflows have strong effects on the pitching moment. Whereas the downward flow reduces the pitching moment, the backward flow tends to increase it. Consequently, the combination effect of these flows makes the variation trend of the pitching moment against the wing kinematic phase more complex. As shown in Figs. 14-17, the sweep angle offset ϕ_0, which is the most effective to control the pitching moment [33], can be either lower or higher than that of the single insect.

As seen in Figs. 14-17, the variations of the power and the wing kinematic coefficients against the phase shift are weakened when the distance *d* becomes larger. A similar trend was exhibited by Maybury and Lehman [41] for the aerodynamics of dragonfly hindwings flapping in the wake of upstream forewings. In the present study, the variations of the following insect's flight parameters depicted in Figs. 14-17 are attributed

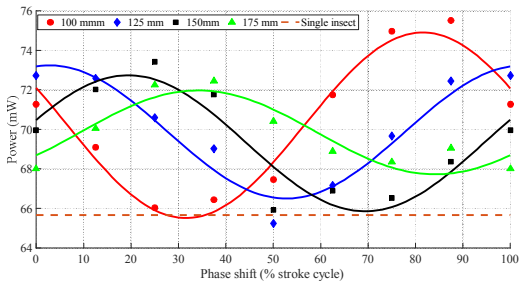

Fig. 18. Sinusoidal functions fitted to the power data.

to the transient wake structures generated by the leading insect's flapping wings. At a large distance, the wake velocities become uniform within fluid and the variations vanish.

It is observed that the variations of the power and wing kinematic coefficients with respect to the phase shift have almost sinusoidal forms. The phases of these sinusoidal functions change as the distance d increases. The power and the sweep angle amplitude ϕ_a show similar trends. This similarity can be explained by the fact that a larger sweep angle amplitude will result in the faster flapping motions of the wings, and thus larger inertial power [42]. Fig. 18 shows sinusoidal functions that are fitted to the data of the mechanical power required for the following insect's trimmed flight. Here, while studying these functions, it is found that when we increase the distance by every 25 mm, the phase of the sinusoidal function is shifted by approximately 20 % of the stroke period. This phase-shifting is attributable to the travel of the strong vortex shed from the leading insect's wings at the start of its downstroke. As the distance increases, the travel time of this vortex until it interferes with the following insect becomes larger. It is widely agreed that wing-wake interaction may have profound impacts on the aerodynamic performance of insect flapping wings [6, 8, 15]. However, in preceding research, scientists mainly paid attention to the interactions between insect wings and their own wakes. In this study, for the first time, the influence of an upstream leading insect's wake on the flight performance of a following counterpart is investigated. According to the phase-shifting data provided by Fig. 18 and the flapping frequency given in Table 2, the average travel velocity of the downstroke starting vortex shed from the leading insect's wings relative to the follower is estimated to be approximately 3 m/s, which is larger than the flight speed of 2.0 m/s. This large velocity is due to the aforementioned backward jet generated by the leading insect to create thrust.

Fig. 19 shows the wake patterns produced by the leading insect during the downstroke of the following insect in the minimum and maximum power cases at a distance d of 100 mm. The wing kinematic phases corresponding to these cases are 25 % and 87.5 %, respectively (Fig. 14). Note that since most of the lift force is generated during the downstroke, we focused only on the downstroke aerodynamics. As shown in Fig. 19, there are two major vortices: the down- and upstroke starting vortices travelling in fluid. These vortices are generated by the leading insect at the beginning of the down- and

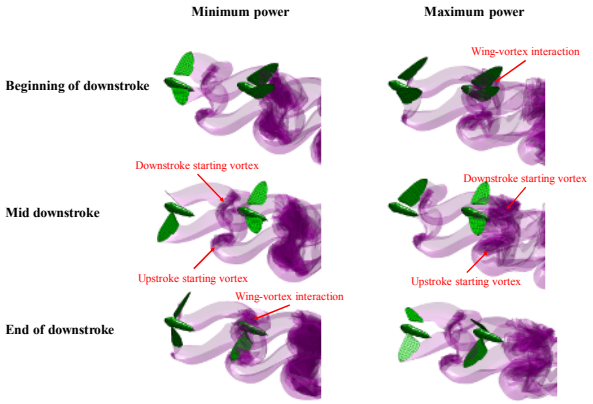

Fig. 19. Wake patterns shed from the leading insect during the downstroke of the following insect at a distance d of 100 mm in the minimum and maximum power cases.

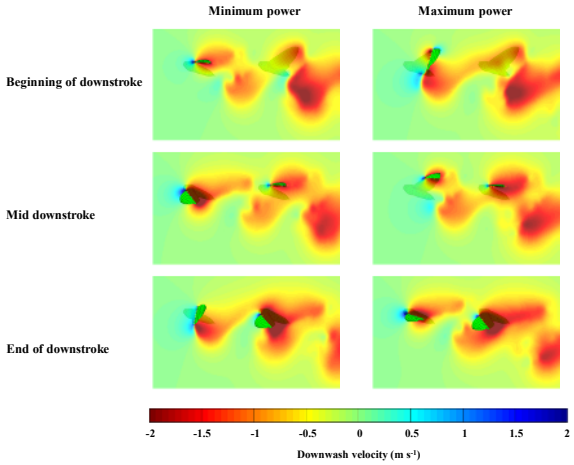

Fig. 20. Downwash wake structures during the downstroke of the following insect at a distance d of 100 mm in the minimum and maximum power cases. A negative sign of the velocity is corresponding to a downward flow.

upstroke, respectively. Whereas the upstroke starting vortex is located well below the following insect and probably has no noticeable effect, the downstroke starting vortex moves downstream and directly impinges on the following insect's wings. Therefore, in this analysis, it was necessary to focus on the interaction between the following insect's wings and the leading insect's downstroke starting vortex. It was found that in the minimum power case, during the course of the downstroke, the starting vortex is located in front of the wings, and the wing-vortex interaction occurs at the end of the downstroke. Based on the physical background provided by Lee and Smith [43], there is a positive effect on the following insect due to a slight induced upward flow region behind the vortex (Fig. 20). So, less power is required in this case, and the following insect can enhance its flight efficiency considerably. On the contrary, in the case of maximum power, the following insect's wings interact with the starting vortex at the beginning of the downstroke. As shown in Fig. 20, the induced downward flow in

front of the following insect appears at the beginning of the downstroke and travels downstream to have a negative effect on the aerodynamic mechanism of the insect. Consequently, the insect needs more power to sustain the trim conditions, and its flight becomes inefficient. The wing-vortex interaction mechanism described in this paper is similar to that of the wake capture effect introduced in the literature [6]. After conducting experimental analyses, Dickinson et al. [6], Birch and Dickinson [15] and Han et al. [8] concluded that during the process of wake capture, a flapping wing can absorb the energy of its own trailing wake to augment the lift. Here, by altering the wing kinematics properly, the following insect also can employ the leader's downstroke starting vortex to improve its own flight performance.

4. Conclusions

This paper has uncovered some important features regarding flapping flight performance in the wake of an upstream leading insect. The two insects were assumed to fly at the same speed of 2.0 m/s with a distance between them varying from 2.2 to 3.9 times of the body length. A potential flow-based aerodynamic model coupling the unsteady panel and the unsteady vortex-lattice methods was employed to simulate the aerodynamics of the insects. To confirm the accuracy of the present model in terms of simulating insect aerodynamics and handling strong wing-wake interaction, the results of a hawkmoth and a dragonfly were validated against Navier-Stokes solutions. The trim conditions of the single insect were found through a gradient-based trim search method, then analyses were conducted to reveal how these trim conditions are affected by the unsteady wake of the leading insect.

When studying aerodynamic force profiles, it was observed that the following insect had almost no influence on the leading insect flight performance. In contrast, noticeable effects were found on the flight characteristics of the following insect. These effects depend on the distance and the wing kinematic phase relationship between the two insects. In general, due to the induced downward flow by the leading insect, the sweep angle amplitude ϕ_a and the required power of the following insect are larger than those of a single insect. Moreover, to compensate for the effect of the induced backward flow by the leading insect, the follower has to reduce its rotation angle offset α_0.

The variations of the required power and wing kinematic coefficients with respect to the change in the phase difference have sinusoidal-like forms. Based on these variation functions, the following insect may choose a proper wing kinematic phase to mitigate the unfavorable effects due to the presence of the leader and then improve its flight efficiency profoundly. The study also revealed that the variations of the required power and the wing kinematic coefficients appear to be weakened with increasing the distance between the two insects. This observation can be explained by the homogenization of the wake velocities at large distances.

The variations of the following insect flight characteristics with respect to the wing kinematic phase are strongly associated with the downstream travel of the leading insect's downstroke starting vortex. It was proved that if the following insect undergoes the downstroke motions when this vortex is approaching, the insect can capture a significant amount of the vortex energy, and hence, minimize its required power. However, if the downstroke motions are carried out when the leading insect's downstroke starting vortex has passed, there will be an opposite effect, and the following insect needs a great deal of power to sustain its flight.

Acknowledgments

This research is funded by Vietnam National Foundation for Science and Technology Development (NAFOSTED) under grant number 107.01-2018.05.

References

[1] W. Shyy, H. Aono, S. K. Chimakurthi, P. Trizila, C. K. Kang, C. E. Cesnik and H. Liu, Recent progress in flapping wing aerodynamics and aeroelasticity, *Progress in Aerospace Sciences*, 46 (7) (2010) 284-327.

[2] J. K. Kim, J. S. Han, J. S. Lee and J. H. Han, Hovering and forward flight of the hawkmoth Manduca sexta: Trim search and 6-DOF dynamic stability characterization, *Bioinspiration & Biomimetics*, 10 (5) (2015) 56012.

[3] H. Liu, S. Ravi, D. Kolomenskiy and H. Tanaka, Biomechanics and biomimetics in insect-inspired flight systems, *Philosophical Transactions of the Royal Society B*, 371 (1704) (2016) 20150390.

[4] A. T. Nguyen, J.-S. Han and J.-H. Han, Effect of body aerodynamics on the dynamic flight stability of the hawkmoth Manduca sexta, *Bioinspiration & Biomimetics*, 12 (1) (2016) 16007.

[5] C. P. Ellington, C. Van den Berg, A. P. Willmott and A. L. R. Thomas, Leading-edge vortices in insect flight, *Nature*, 384 (6610) (1996) 626-630.

[6] M. H. Dickinson, F. O. Lehmann and S. P. Sane, Wing rotation and the aerodynamics basis of insect flight, *Science*, 284 (5422) (1999) 1954-1960.

[7] S. P. Sane and M. H. Dickinson, The aerodynamic effects of wing rotation and a revised quasi-steady model of flapping flight, *J. of Experimental Biology*, 205 (8) (2002) 1087-1096, http://jeb.biologists.org/content/205/8/1087.

[8] J. S. Han, J. W. Chang, J. K. Kim and J. H. Han, Role of trailing-edge vortices on the hawkmothlike flapping wing, *J. of Aircraft*, 52 (4) (2015) 1256-1266.

[9] V. M. Ortega-Jimenez, J. S. M. Greeter, R. Mittal and T. L. Hedrick, Hawkmoth flight stability in turbulent vortex streets, *J. of Experimental Biology*, 216 (2013) 4567-4579.

[10] S. Ravi, J. D. Crall, A. Fisher and S. A. Combes, Rolling with the flow: bumblebees flying in unsteady wakes, *J. of Experimental Biology*, 216 (2013) 4299-4309.

[11] J. T. Vance, I. Faruque and J. S. Humbert, Kinematic strategies for mitigating gust perturbations in insects, *Bioinspiration & Biomimetics*, 8 (1) (2013) 16004.

[12] K. Warfvinge, M. Kleinheerenbrink and A. Hedenstro, The power-speed relationship is U-shaped in two free-flying hawkmoths (Manduca sexta), *J. of The Royal Society Interface*, 14 (134) (2017) 20170372.

[13] A. P. Willmott and C. P. Ellington, The mechanics of flight in the hawkmoth Manduca sexta: I. Kinematics of hovering and forward flight, *J. of Experimental Biology*, 200 (21) (1997) 2705-2722.

[14] H. Liu and H. Aono, Size effects on insect hovering aerodynamics: an integrated computational study, *Bioinspiration & Biomimetics*, 4 (1) (2009) 15002.

[15] J. M. Birch, The influence of wing-wake interactions on the production of aerodynamic forces in flapping flight, *J. of Experimental Biology*, 206 (13) (2003) 2257-2272.

[16] Y. Ryu, J. W. Chang, J. Chung and D. Kim, Experimental investigation of flexible hawkmoth-like wings on the wing-wake interaction in hovering flight, *J. of Bionic Engineering*, 15 (1) (2018) 139-153.

[17] K. Senda, T. Obara, M. Kitamura, N. Yokoyama, N. Hirai and M. Iima, Effects of structural flexibility of wings in flapping flight of butterfly, *Bioinspiration & Biomimetics*, 7 (2) (2012) 25002.

[18] J. E. Bluman, M. K. Sridhar and C. Kang, The influence of wing flexibility on the stability of a biomimetic flapping wing micro air vehicle in hover, *57th AIAA/ASCE/AHS/ASC Structures, Structural Dynamics, and Materials Conference*, San Diego, California, USA (2016) 0470.

[19] S. Kauertz, F. Holzäpfel and J. Kladetzke, Wake vortex encounter risk assessment for crosswind departures, *J. of Aircraft*, 49 (1) (2012) 281-291.

[20] D. Bieniek, R. Luckner, I. De Visscher and G. Winckelmans, Simulation methods for aircraft encounters with deformed wake vortices, *J. of Aircraft*, 53 (1) (2016) 1581-1596.

[21] C. P. Ellington, The aerodynamics of hovering insect flight: II. Morphological parameters, *Philosophical Transactions of the Royal Society B*, 305 (1984) 17-40.

[22] R. P. O'Hara and A. N. Palazotto, The morphological characterization of the forewing of the Manduca sexta species for the application of biomimetic flapping wing micro air vehicles, *Bioinspiration & Biomimetics*, 7 (4) (2012) 46011.

[23] A. P. Willmott, *The Mechanics of Hawkmoth Flight*, Ph.D. Dissertation, Dept. of Zoology, Univ. of Cambridge, UK (1995).

[24] J. Katz and A. Plotkin, *Low-speed Aerodynamics from Wing Theory to Panel Methods*, 2nd Ed., Cambridge University Press, New York, USA (2001).

[25] B. A. Roccia, S. Preidikman, J. C. Massa and D. T. Mook, Modified unsteady vortex-lattice method to study flapping wings in hover flight, *AIAA J.*, 51 (11) (2013) 2628-2642.

[26] A. T. Nguyen, J.-K. Kim, J.-S. Han and J.-H. Han, Extended unsteady vortex-lattice method for insect flapping wings, *J. of Aircraft*, 53 (6) (2016) 1709-1718.

[27] J.-H. Han and A. T. Nguyen, Dynamic stability of flapping-wing micro air vehicles with unsteady aerodynamic model, *ASME 2017 Fluids Engineering Division Summer Meeting*, Waikoloa, Hawaii, USA (2017) V01AT01A002.

[28] A. T. Nguyen and J.-H. Han, Modified unsteady vortex lattice method for aerodynamics of flapping wing models, *ASME/JSME/KSME 2015 Joint Fluids Engineering Conference*, Seoul, South Korea (2015) V01AT04A001.

[29] H. Liu, C. Ellington, K. Kawachi, C. Van Den Berg and A. P. Willmott, A computational fluid dynamic study of hawkmoth hovering, *J. of Experimental Biology*, 201 (4) (1998) 461-477.

[30] E. C. Polhamus, Predictions of vortex-lift characteristics by a leading-edge suction analogy, *J. of Aircraft,* 8 (4) (1971) 193-199.

[31] M. Ramasamy and J. G. Leishman, A Reynolds number-based blade tip vortex model, *J. of the American Helicopter Society*, 52 (3) (2007) 214-223.

[32] F. Gandhi and L. Tauszig, A critical evaluation of various approaches for the numerical detection of helicopter blade-vortex interactions, *J. of the American Helicopter Society*, 45 (3) (2000) 179-190.

[33] J. K. Kim and J. H. Han, Control effectiveness analysis of the hawkmoth Manduca sexta: A multibody dynamics approach, *International J. of Aeronautical and Space Sciences*, 14 (2) (2013) 152-161.

[34] A. T. Nguyen and J. H. Han, Wing flexibility effects on the flight performance of an insect-like flapping-wing micro-air vehicle, *Aerospace Science and Technology*, 79 (2018) 468-481.

[35] H. Aono, W. Shyy and H. Liu, Near wake vortex dynamics of a hovering hawkmoth, *Acta Mechanica Sinica*, 25 (2009) 23-36.

[36] K. B. Lua, K. C. Lai, T. T. Lim and K. S. Yeo, On the aerodynamic characteristics of hovering rigid and flexible hawkmoth-like wings, *Experiments in Fluids*, 49 (6) (2010) 1263-1291.

[37] J. K. Wang and M. A. Sun, Computational study of the aerodynamics and forewing - hindwing interaction of a model dragonfly in forward flight, *J. of Experimental Biology*, 208 (19) (2005) 3785-3804.

[38] M. Sun and S. L. Lan, A computational study of the aerodynamic forces and power requirements of dragonfly (Aeschna juncea) hovering, *J. of Experimental Biology*, 207 (11) (2004) 1887-1901.

[39] T. M. Casey, A comparison of mechanical and energetic estimates of flight cost for hovering sphinx moths, *J. of Experimental Biology*, 91 (1) (1981) 117-129.

[40] M. Sun and J. Tang, Lift and power requirements of hovering flight in Drosophila virilis, *J. of Experimental Biology*, 205 (16) (2002) 2413-2427.

[41] W. J. Maybury and F. Lehmann, The fluid dynamics of flight control by kinematic phase lag variation between two robotic insect wings, *J. of Experimental Biology*, 207 (26)

(2004) 4707-4726.
[42] A. P. Willmott and C. P. Ellington, The mechanics of flight in the hawkmoth Manduca sexta: II. Aerodynamic consequences of kinematic and morphological variation, *J. of Experimental Biology*, 200 (21) (1997) 2723-2745.
[43] D. J. Lee and C. A. Smith, Effect of vortex core distortion on blade-vortex interaction, *AIAA J.*, 29 (9) (1991) 1355-1362.

Anh Tuan Nguyen is a lecturer at the Faculty of Aerospace Engineering, Le Quy Don Technical University, Ha Noi, Vietnam. He received his Ph.D. in aerospace engineering from KAIST, Daejeon, S. Korea, in 2017. His research interests are bioinspired flapping-wing micro air vehicles, unsteady aerodynamics, multibody dynamics and aeroelasticity.

Thanh Dong Pham is a lecturer at the Faculty of Aerospace Engineering, Le Quy Don Technical University, Ha Noi, Vietnam. He received the Master of Science in Russia in 2012. His research interests are aerodynamics of rotor machines, unsteady aerodynamics and multibody dynamics.

Quoc Tru Vu is an Associate Professor at the Faculty of Aerospace Engineering, Le Quy Don Technical University, Ha Noi, Vietnam. He received the Ph.D. from Le Quy Don Technical University in 2002. His research interests are aircraft system design, aircraft structure, unsteady aerodynamics and aeroelasticity.